Morris Shatzkes Moshe Av-Ron Robert A. Gdula

Defect-Related Breakdown and Conduction in SiO,

A statistical model incorporating the effects of defects provides a good representation of breakdown results for Al-SiO $_2$ -Si MOS capacitors. Implications of this model for interpretation of the yield from life tests and histograms obtained from ramp tests are discussed for the case of a Poisson distribution of defects over the capacitors. The breakdown rates of MOS capacitors in life tests are found to be correlated to defects inferred from conduction measurements.

Introduction

The major role of the gate insulator in MOSFETs is to allow for the application of an electric field normal to the surface of the semiconductor; however, there must be negligible current through the gate insulator. Associated with this role is a failure mode: dielectric breakdown of the gate insulator (i.e., a collapse of the dielectric strength of the gate insulator), a situation that terminates the activity of the device. Among the various dielectrics available, the material most frequently used for gate insulators is silicon dioxide (SiO₂), chosen because of its excellent electrical properties, remarkable stability, and compatibility with silicon technologies currently used in the microelectronics industry. Breakdowns in SiO2, reviewed recently by Solomon [1], are classified as either high-field intrinsic events or low-field defect-related phenomena. The latter, though of greater technological importance, are understood less than the intrinsic events and are the subject of this paper.

Various techniques have been used to detect defects in insulators [2], including the use of liquid crystals for the detection of "hot spots" (regions of high current density in gate insulators) [3], scanning internal photoemission [4, 5], and scanning internal photovoltage [6, 7]. Recently, we have found that defects at $Al-SiO_2$ interfaces can be inferred from deviations of the current-voltage (*I-V*) characteristics of $Al-SiO_2$ -Si MOS capacitors [8]. Two kinds of defects could be distinguished. At low fields, we sometimes found a component of current whose field de-

pendence was not reconcilable with any of the electrode-limited models known to us and whose temperature dependence was stronger than that associated with field emission. At intermediate fields, another component of excess current was found: one that followed the field and temperature dependence appropriate for field emission, but that had a lower barrier height. The defect-free Al-SiO₂ interfacial barrier height ϕ_0 is 3.19 eV and analysis of the excess current at intermediate fields provides a lower Al-SiO₂ barrier height ϕ_1 (2.43 \pm 0.09 eV) characteristic of the defect. The fractional area covered by the defect can also be obtained from the data. The lack of correlation between deviations in the intermediate- and low-field regions and the different temperature and field dependencies imply two different types of defects.

The use of *I-V* characteristics to determine the existence of defects has advantages over other techniques. First, the strong exponential dependence of the current on the interfacial barrier height provides extreme sensitivity *vis-à-vis* inhomogeneities of interfacial barrier heights, and thus allows the detection of even very small areas of such regions. Second, the measurements can also be carried out on simple MOS capacitors, thus eliminating the need for special structures.

This study was carried out in two phases. First, we obtained *I-V* characteristics of Al-SiO₂-Si MOS capacitors with dry thermal SiO₂ grown at 1200°, 1000°, and 850°C.

Copyright 1980 by International Business Machines Corporation. Copying is permitted without payment of royalty provided that (1) each reproduction is done without alteration and (2) the *Journal* reference and IBM copyright notice are included on the first page. The title and abstract may be used without further permission in computer-based and other information-service systems. Permission to *republish* other excerpts should be obtained from the Editor.

469

This provided a distribution of the two defects over the capacitors. Subsequently, the MOS capacitors were subjected to field-temperature stress tests, during which the times to breakdown were monitored. Our objective was to determine whether any correlation existed between the incidence of defects and the times to breakdown; the results suggest that this is the case. Early breakdown (commonly referred to as "time-zero" breakdown) may be related to defects associated with low-field current deviations, whereas longer mean times to breakdown are found for smaller areas of interfacial inhomogeneity. We find that densities of the interfacial inhomogeneities decrease with increasing oxidation temperature [9]. Consistent with this finding, similar samples, after subjection to fieldtemperature stress, showed mean times to breakdown that increased with increasing oxidation temperature.

The results of these field-temperature stress tests (life tests) are consistent with breakdown events being random and a dependency of the lifetime on the defect area. In contrast with previous notions, we find no need to invoke wearout mechanisms [10, 11]. A steep rise in a plot of the cumulative number of MOS capacitors breaking down as a function of the logarithm of the time is expected from a statistical model (discussed later).

The usual procedure [1] for obtaining defect densities is to equate the fraction of MOS capacitors surviving a breakdown test to the negative exponential of the area of the MOS capacitor times the defect density. This assumes a Poisson distribution of defects and results in a defect density that depends on the field and the duration of the test. In reality, these tests provide breakdown densities (i.e., the density of defects that break down during the test) rather than the required defect density. Our procedure provides both the defect densities (from conduction measurements) and the breakdown times (from field-temperature life tests).

Much confusion exists concerning the dependence of defect-related breakdown events on processing. As pointed out by Solomon [1], the values of defect densities obtained from an experiment depend on the nature of the experiment, the quality or initial state of the wafers, the cleaning procedures, the various preoxidation treatments [12], the oxidation conditions, the cleanliness of the furnace, the techniques of electrode deposition, and the various annealing treatments. Thus, it may not be too surprising that the lower defect densities we obtained at higher oxidation temperatures are contrary to those reported by Osburn and Ormond [13]. A possible cause for this discrepancy is that at higher oxidation temperatures the cleanliness of the furnace becomes more critical. To obtain our results for the 1200°C oxidation, the furnace was

cleaned with HCl (see details in the section on experimental procedures). In the absence of this step, MOS capacitors with oxides grown at 1200°C showed large defect densities.

Experimental procedures

Single-crystal silicon wafers, $\langle 100 \rangle$ p-type boron-doped (ρ \approx 15 Ω -cm), were cleaned and then thermally oxidized at ambient oxidation temperatures $T_{\rm ox}$ of 1200°, 1000°, and 850°C in a single-walled fused silica tube that had been HCl cleaned to nominal thicknesses of 100, 36, and 25 nm, respectively. The HCl cleaning consisted of running a 5% HCl/95% O, gas mixture through the tube at the oxidation temperature for 2 h and then purging overnight in dry O_a (≈ 16 h) immediately prior to the oxidation run. The wafers were subsequently annealed in situ at the corresponding temperatures for 20, 35, and 245 min in a nitrogen environment. For a few wafers with oxide grown at 1200°C, the 100-nm oxide film was then chemically etched back to a nominal thickness of 36 nm in order to prevent impact ionization in the oxide during high-field conduction measurements [14]. In a separate run, similar wafers were oxidized to a nominal film thickness of 100 nm, at 1000°C for 180 min, followed by an in situ 30min post-oxidation anneal.

Aluminum electrodes 100 nm thick were deposited by e-gun via metal masks with nominal areas of 0.057, 0.20, and 1.85 mm². An ≈500-nm-thick layer of aluminum was deposited on the back side of the wafers to improve ohmic contact to the silicon. After metallization, the wafers were annealed for 20 min at 400°C in a 90% N_s/10% H, environment. This annealing step eliminates charge and surface states introduced during e-gun deposition of Al [15]. It has been reported that Al penetrates the oxide at annealing temperatures ≥500°C [16, 17]. In another study [18], the oxide transport properties were unaffected by high Al concentrations; identical results were obtained for Al-SiO₂-Si MOS capacitors unannealed or annealed at 500° and 550°C for 20 min. If significant penetration did occur during the 400°C anneal, our results could presumably be influenced by the presence of Al and thus may not reflect the properties of pure SiO2. However, to our knowledge, no experimental evidence exists for such penetration at 400°C.

Oxide thicknesses were determined from ellipsometric and capacitance measurements; a refractive index of 1.465 and a low-frequency dielectric constant of 3.9 were assumed. The actual electrode areas A were determined from measurements of the diameters of the electrodes with a micrometer-calibrated microscope. After the postmetallization anneal, we measured (via the I-V loop method [19]) a mobile-charge density in the oxide of $\leq 6.8 \times 10^7/\text{mm}^2$.

The room-temperature high-frequency capacitancevoltage (C-V) curves were obtained in a configuration similar to that outlined by Grove et al. [20]. The flatband voltage shift for a charge-free oxide is a known function of the substrate doping and of the difference between the barrier heights for Al-SiO₂ (3.2 eV) [21] and Si-SiO₃ (3.1 eV from the Si conduction band) [22]. For our samples this shift was calculated to be 0.8 V for T = 300 K. We accepted only capacitors whose flatband voltage shift was within 0.05 V of this value. Details concerning measurements of the I-V characteristics of the MOS capacitors are given in Ref. [14] and are not repeated here. For the field-temperature stress tests, the Al-SiO₂-Si MOS capacitors with electrode areas equal to 0.2 mm² were stressed on a temperature-controlled multiple-probe stage assembly. The stressed capacitors were connected, each through a separate 1-M Ω series resistor, to a common voltage source. Breakdown of any given capacitor was defined when the current through that capacitor exceeded 1 μ A, as determined from the voltage drop across the corresponding series resistor. These voltage drops were monitored to provide the times to breakdown for individual MOS capacitors. Due to limitations in time resolution, all breakdown events that occurred within the first 6 min were lumped into a "time-zero" breakdown category.

All MOS capacitors were screened prior to the application of the field-temperature stress test to eliminate those capacitors with gross defects. This screening was done by applying 400 MV/m for about an hour at room temperature prior to increasing the temperature.

Results and analysis

Features of the I-V characteristics of $Al\text{-}SiO_2\text{-}Si(p)$ MOS capacitors (Al electrode biased negatively) can be used to provide information concerning oxide-related defects. If a defect affects the current and if the fractional effective area of the defect fluctuates from sample to sample, the observed currents should fluctuate correspondingly. Thus, variations in the observed currents among various MOS capacitors could be used to signify the presence and type of defects. We identified two types of defects.

In the course of the conduction measurements, we found a component of current at low fields that could not be explained by our generalized model, even with the interfacial inhomogeneities. This component of current exhibited an abnormally high temperature dependence and an abnormally low field dependence. Thus, we attribute this component of current to a defect distinct from the interfacial inhomogeneity and denote it as a tail defect. We also often found that capacitors having high currents at low fields break down within an exceedingly short time compared to those not exhibiting such currents, suggest-

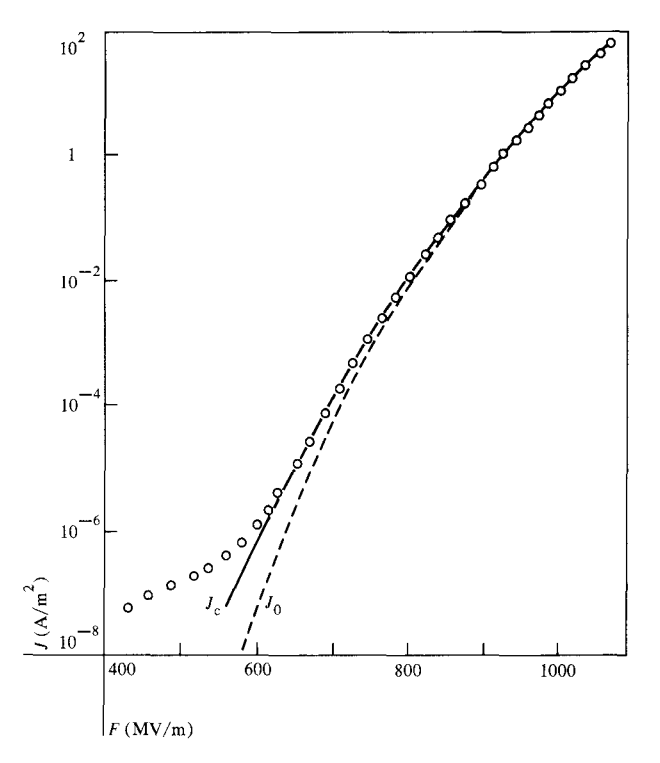


Figure 1 Current density *J vs.* field *F* for T = 350 K; $\alpha = 4.04 \times 10^{-6}$, $\phi_0 = 3.19$ eV, $\phi_1 = 2.43$ eV.

ing a causal relation between tail defects and early (time-zero) breakdown found in the field-temperature stress tests.

From variations of the *I-V* characteristics at fields F in the range of $\approx 600\text{--}800$ MV/m, one type of defect is characterized as an interfacial barrier inhomogeneity. If we consider an MOS capacitor with a homogeneous Al-SiO₂ interfacial barrier height ϕ_0 of 3.19 eV to contain an interfacial inhomogeneity characterized by a lower barrier height ϕ_1 and a fractional effective area α , the experimentally observed current density J, assumed to be a superposition of the two components, can be written as a composite current density

$$J_c = (1 - \alpha)J_0 + \alpha J_1. \tag{1}$$

Here, J_0 and J_1 are the current densities $J(\phi)$ obtained from the Murphy-Good theory for currents injected from a metal electrode into a vacuum [23], generalized to the case where the vacuum is replaced by an insulator with a Franz-type dispersion relation [24]. Thus, $J(\phi)$ gives J_0 for $\phi = \phi_0$ and J_1 for $\phi = \phi_1$. This superposition is an excellent representation of the experimental results for $\phi_0 = 3.19$ and $\phi_1 = 2.43$ eV (see for example Fig. 1). We found other parameters of the generalized model pertaining to properties of the SiO₂ to be invariant with the interfacial inhomogeneity [8].

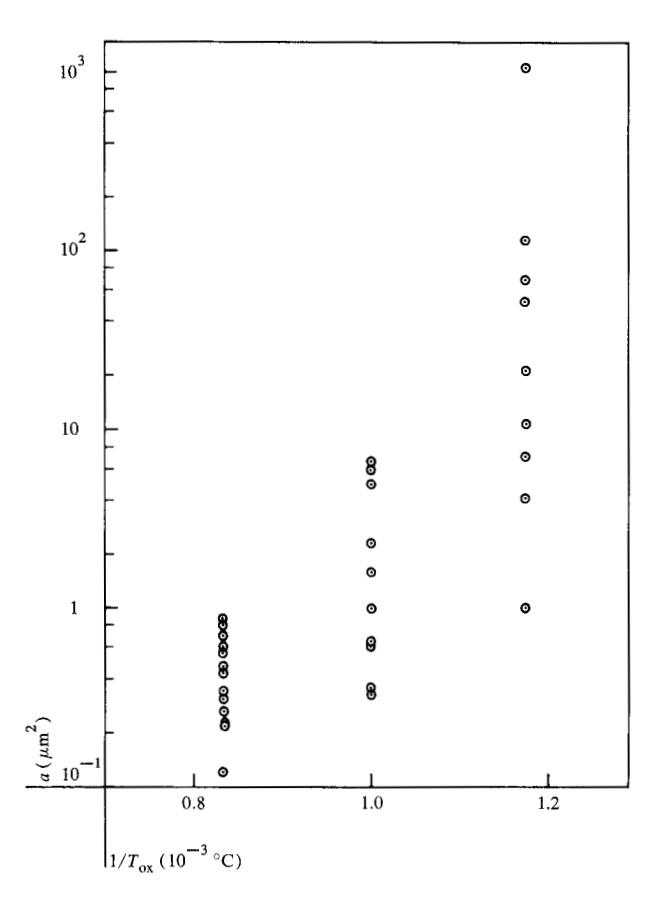


Figure 2 Distribution of defect areas a, normalized to $A = 0.20 \text{ mm}^2$, as a function of the inverse of T_{ox} .

Table 1 Effective area a (in μ m²) associated with ϕ_1 as a function of the oxidation temperature for nominal oxide film thicknesses as indicated.

$T_{\rm ox} = 1200^{\circ}C$ film thickness = 36 nm ¹	1000° C	$850^{\circ} C$ $25 nm^2$	
film thickness = 36 nm ¹	$36 nm^2$		
0.122	0.0914	0.254	
0.223	0.163^4	1.794	
0.229	0.329	2.714	
0.262	0.581^4	4.16	
0.313	0.627	21.6	
0.341	1.00	52.1	
0.43	1.60	69.4	
0.44	1.68^{4}	115.4	
0.442	2.33	1070.0	
0.473^{3}	2.36		
0.579	4.99		
0.616	5.88		
0.711			
0.807^{3}			
0.886			

¹After etch-back

Figure 1 shows the experimental results of current density vs. field (data points), the current density J_0 computed with the mean values of the parameters pertaining to the generalized model (- - -), and the composite current density J_c (-----). For this sample $\alpha = 4.04 \times 10^{-6}$. At low fields (≤ 600 MV/m) the experimental data show a clear change of trend.

Table 1 lists the effective areas associated with ϕ_1 for the three oxidation temperatures $T_{\rm ox}$. Unless otherwise specified, the nominal area of the Al electrode is 0.2 mm², $\phi_1 = 2.43 \pm 0.09$ eV, and the nominal oxide film thicknesses are as follows $[T_{\rm ox}\,(^{\circ}{\rm C}),$ thickness (nm)]: 1200, 36; 1000, 36; 850, 25.

The mean area \bar{a} and the standard deviation σ of the inhomogeneities associated with $T_{ox} = 1200^{\circ}\text{C}$, \bar{a}_{1200} and σ_{1200} , are 0.485 μ m² and 0.224 μ m², respectively; $(\sigma_{1200})^2/\bar{a}_{1200} = 0.11 \ \mu\text{m}^2$, and since this is smaller than the smallest a_{1200} $(a = \alpha A)$, the ensemble can be normalized to obey a Poisson distribution, a notion that conveys randomness. The inhomogeneities associated with T_{ox} = 1000°C are averaged as two separate subsets, in accordance with the area of the respective electrodes A_1 , A_2 (A_1 = 0.2 mm², $A_S = 0.05$ mm²). For the larger-area electrode (denoted by L) $\bar{a}_{1000} = 2.39 \,\mu\text{m}^2$ and $\sigma_{1000} = 2.02 \,\mu\text{m}^2$. For the smaller-area electrode (denoted by S), $\tilde{a}_{1000} =$ 0.629 μm^2 and $\sigma_{1000} = 0.733 \ \mu \text{m}^2$. It turns out that the ratio of $(\bar{a}_{1000})_{\rm L}/(\bar{a}_{1000})_{\rm S} \approx A_{\rm L}/A_{\rm S}$. Here, because $[(\sigma_{1000})^2/\tilde{a}_{1000}]_L \approx 1.7 \ \mu\text{m}^2$ and is larger than the smallest $(a_{1000})_1$, (0.33 μ m²), we can only say that the sample size is too small to allow determination of whether the distribution is indeed random. The inhomogeneities associated with the 850°C oxidation are found to have areas distributed over several orders of magnitude. When averaged, this ensemble provides a mean area \bar{a}_{850} that is heavily weighted by the larger inhomogeneity areas and therefore misrepresents the distribution. For this reason, we avoid the exercise altogether.

Assuming that the effective area of an inhomogeneity in a given MOS capacitor scales with the electrode area, the data given in Table 1 are now normalized to the 0.2-mm² electrode and are presented in Fig. 2 as a function of the inverse of the oxidation temperature. Let $D(a_{T_{\rm ox}})$ be the distribution of the effective area of the inhomogeneities associated with an oxidation temperature $T_{\rm ox}$. The effect of $T_{\rm ox}$ on $D(a_{T_{\rm ox}})$ is marked, particularly for the upper limits of these distributions. Although the variation of $D(a_{T_{\rm ox}})$ with $T_{\rm ox}$ is of considerable interest, more intriguing is the fact that almost the entire range of areas is reasonably well accounted for by a single mean lower barrier height $\bar{\phi}_1 = 2.43$ eV. This finding is indicative of a definite structure that characterizes these inhomogeneities.

As-grown.

³Film thickness of oxide is 90 nm.

⁴Nominal area of Al electrode is 0.057 mm².

Figure 3 illustrates some general current trends for Al-SiO₂-Si(p) MOS capacitors with oxides grown at 1200° C and etched back to a nominal thickness of 36 nm for fields F = 500-800 MV/m and ambient device temperatures T = 300-575 K. Given here as solid curves are the calculated loci of $J_o(T, F)$ and $J_o(T, F)$ for

$$J_{c} = (1 - \tilde{\alpha} - 2\sigma)J_{0} + (\tilde{\alpha} + 2\sigma)J_{1}, \tag{2}$$

with J_0 and J_1 as defined earlier; $\tilde{\alpha}$ and σ are the mean fractional area and standard deviation associated with ϕ , and are given by 2.71×10^{-6} and 1.11×10^{-6} , respectively. The data points shown are the experimental current densities J(T, F); the dashed lines indicate trends. Some data at 500 and 600 MV/m, which would mainly illustrate the variability of the experimental currents, were omitted from the figure to avoid clutter. At 800 MV/m (\bigcirc) the J values fall within the region bounded by J_0 and J_0 for the entire range of ambient temperatures. At 700 (△) and 600 MV/m (\square , \blacksquare) the temperature dependence of J is stronger than that of J_c . At 500 MV/m (\bigcirc , \bullet) the temperature at which the J values exceed J_c is generally lower. At 500 MV/m the J values are larger than J_c at all the temperatures used. (Shading of the data points indicates that only a single sample was used for all temperatures while the open symbols indicate a discrete sample.) This behavior is indicative of a component of current that dominates at low fields and that has a stronger temperature dependence than that predicted by the generalized model of field emission.

Results of field-temperature tests for MOS capacitors with dry thermal $\mathrm{SiO_2}$ grown at 1200° and $1000^\circ\mathrm{C}$ (nominal film thickness of 100 nm) are summarized in Table 2. These MOS capacitors, with a total of 38 units in each ensemble, were stressed at a stress temperature T_{st} of 500 K at 400 MV/m (negative polarity applied to the Al electrodes). Figure 4 shows the cumulative number of breakdown events (disregarding "time-zero" failures) as a function of the time t.

The distributions of times to breakdown, obtained from the field-temperature stress test (life-test) results, can be understood in terms of a statistical multinomial model. The assumption here is that any given ensemble of N MOS capacitors consists of i subsets, $i = 1, \dots, K$, each subset having N_i members, such that $N = \sum_{i=1}^{K} N_i$. Now, let $p_i(t)$ be the probability that a capacitor of type i will break down within time t. The probability that n capacitors will break down within t is

$$p_i^{n_i}(t) = \sum_{\sum_{n_i = n}} \prod_{i=1}^K \binom{N_i}{n_i} p_i^{n_i}(t) [1 - p_i(t)]^{N_i - n_i},$$
 (3)

where the sum is over all distinct integer solutions of $\sum_{i=1}^{K} n_i = n$. The expectation value for the number of

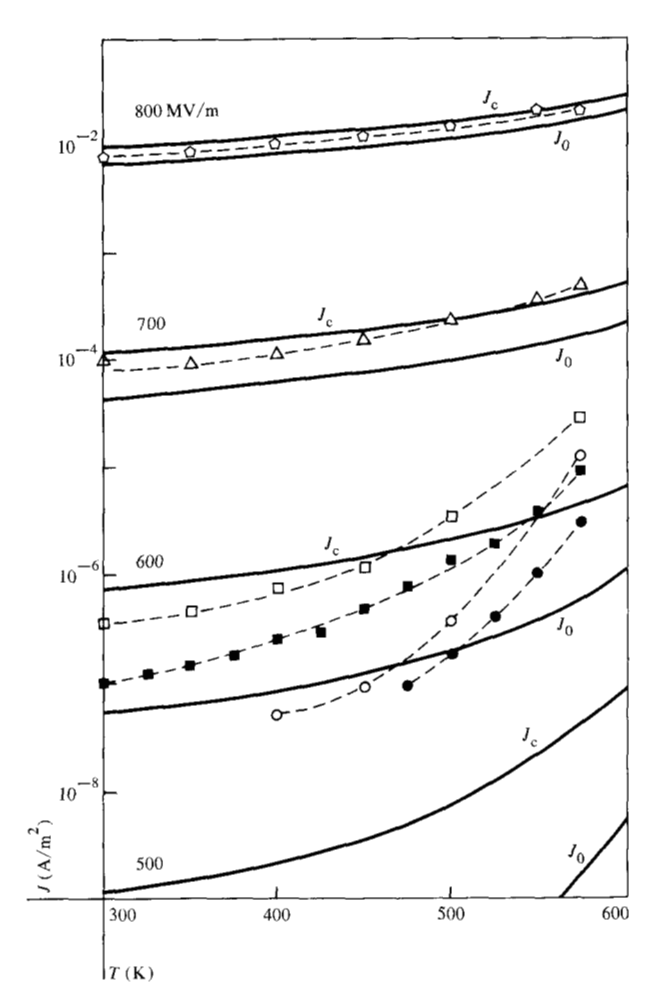


Figure 3 Ambient temperature T dependence of the current density. Solid lines are computed; see Eq. (2) and text. Data points are for F (MV/m) of 500 (\bigcirc , \blacksquare), 600 (\square , \blacksquare), 700 (\triangle), and 800 (\bigcirc). Shading of the data points indicates that only a single sample was used for all temperatures, while the open symbols indicate a discrete sample.

Table 2 Results of field-temperature stress tests on MOS capacitors with dry thermal SiO_2 grown to 100 nm; $T_{\rm st}=500~{\rm K}$, $F=400~{\rm MV/m}$.

Oxidation	Number	Number	
temperature (°C)	$0-0.1 \ h^{1}$	$0.1 h-end^2$	surviving
1200	6	9	23
1000	15	4	9

¹Includes screening failures (room temperature) and "time-zero" breakdowns (500 K). ²1950 h for $T_{\rm ex}=1200^{\circ}{\rm C}$; 1000 h for 1000°C.

capacitors breaking down within t is

$$\langle n(t) \rangle = \sum_{i=1}^{K} N_i p_i(t),$$
 (4)

473

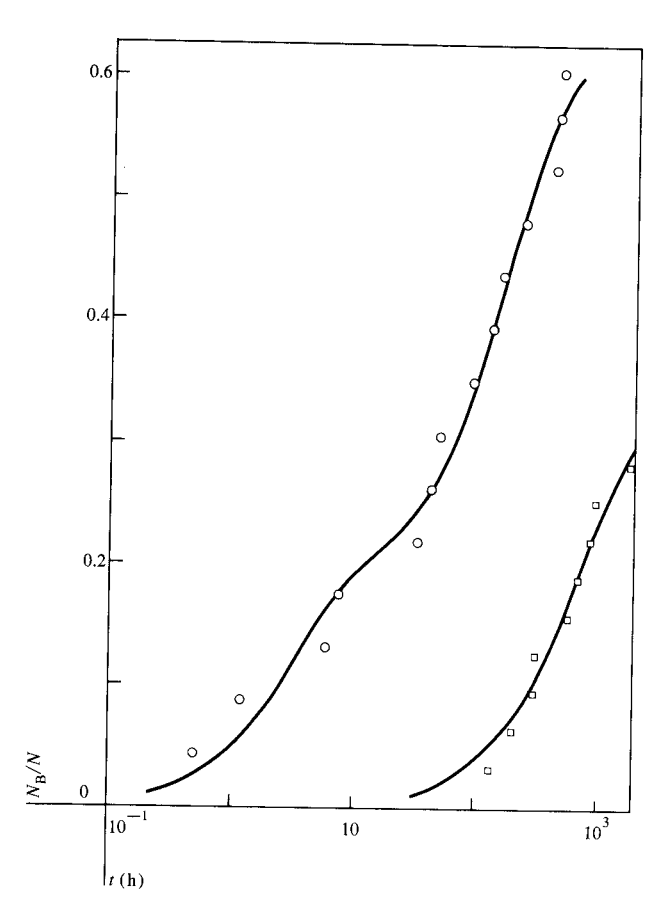


Figure 4 Cumulative number of breakdown events $N_{\rm B}/N$ for MOS capacitors for $T_{\rm ox}=1000^{\circ}\,(\odot)$ and $1200^{\circ}{\rm C}\,(\Box)\,\nu s$. time to breakdown t. The curves represent the fit of Eq. (4) to the data with parameters as discussed in the text.

Table 3 Results of field-temperature stress tests on MOS capacitors with thin oxide films; $T_{\rm st}=500~{\rm K}$, $F=400~{\rm MV/m}$.

1200	1000	850
36¹		25 ²
38	76	75
20	33	17
1	8	21
11	24	35
6	10	0
	36 ¹ 38	36 ¹ 36 ² 38 76 20 33 1 8 11 24

After etch-back

 $^{3}500 \text{ h for } T_{\text{ex}} = 1200^{\circ} \text{ and } 1000^{\circ}\text{C}; 182 \text{ h for } 850^{\circ}\text{C}.$

and the mean square deviation is

$$\sigma^2 = \sum_{i=1}^K N_i p_i(t) [1 - p_i(t)].$$
 (5)

Assuming the breakdown events occur randomly, the form chosen for $p_i(t)$ is

$$p_i(t) = 1 - \exp(-t/\tau_i),$$
 (6)

where τ_i is the mean time characteristic of the *i*th subset.

Returning to Fig. 4, let B(t) be the experimentally observed number of breakdown events that occur within t. The curve associated with the 1000° C breakdown data was obtained by a least-squares fit of

$$\langle n(t) \rangle = N_1 [1 - \exp(-t/\tau_1)] + N_2 [1 - \exp(-t/\tau_2)]$$

to the experimental data, with N_1 , N_2 , τ_1 , and τ_2 being 4, 10, 3.1 h, and 194.5 h, respectively. This fitting was done iteratively, such that

$$\left\{ \sum_{t} \left[\langle n(t) \rangle - B(t) \right]^{2} (NDP - 1)^{-1} \right\}^{1/2} \to 0, \tag{7}$$

where NDP is the number of data points under consideration. The curve associated with the 1200°C oxidation data was obtained in a similar manner, with N_1 , N_2 , τ_1 , and τ_2 being 6, 5, 616 h, and 1413 h, respectively. This result suggests, for the two subsets, a total of 11 breakdown events, whereas up to 1950 h we observed only 9 events. The implication here is that the test was terminated before the last two events occurred; these are expected at ≈ 2500 and 10^4 h. Considering the number of capacitors that did not fail upon termination of the stress test (Table 2), the supposition is that the remaining capacitors are associated with larger characteristic breakdown times.

Results of field-temperature stress tests of MOS capacitors with thin oxide films are summarized in Table 3. All capacitors were stressed at 500 K at 400 MV/m (negative polarity applied to the Al electrodes).

Figure 5 shows the cumulative numbers of breakdown events associated with the etched-back 1200° C films (\square), and the as-grown 1000° (\bigcirc) and 850° C (\triangle) thin-oxide films. Also shown are three curves describing the expectation values of times to breakdown. The expectation curves associated with the 1200° and 1000° C data were calculated using Eqs. (4) and (6) for K=3, while for the 850° C case we used K=2. The deviation between each of the curves and the corresponding experimental data was calculated from Eq. (7). The values for N_i , T_i , and the deviation σ for the three data sets are given in Table 4.

For the 1000° C set, we did not have the times for the early breakdown events; however, we used the shape of the available data, together with Eq. (7), to calculate the expectation curve. Thus, we can account for most of the early failures. The expectation curve for the 1200° C data was calculated with $\sum_{i=1}^{3} N_i = 13$, whereas up to 500 h we

observed only 11 breakdown events. The explanation for this discrepancy is as discussed earlier; see Table 3.

For the MOS capacitors with the 36-nm (after etchback) oxide films grown at 1200°C, we extended the screening process by measuring the current at 600 MV/m for 100 s at room temperature before the conventional screen. The choice of 600 MV/m was made so that we could measure currents even in MOS capacitors containing small defects. As it turned out, those capacitors showing excessively high currents failed within this 100 s of current measurement. The remaining capacitors showed no breakdown when subsequently put through standard screening; when they were put through the field-temperature stress test, only a single early breakdown occurred. Referring to Table 3 (the 1200°C oxidation temperature group), out of 18 capacitors on stress test only one had an early breakdown, compared with 8 breakdowns out of 43 and 21 out of 58 for the 1000° and 850°C groups, respectively. This supports our hypothesis that early breakdowns and tail defects are related. The fact that we were able to measure high-field I-V characteristics of MOS capacitors with tail defects at all is probably due to our technique of using pulses of short duration.

Discussion

Oxide quality is often determined from life tests and is quantified in terms of a defect density [1]. Another method is the ramp test [1], where the applied field is a linear function of the time and the breakdown probability density is presented as a function of the field. The statistical model has implications concerning each of these measures of oxide quality.

To be definite, and so that explicit results can be obtained, assume a Poisson distribution for the defects. The probability that a capacitor has n defects is then $e^{-\mu}\mu^n/n!$, μ being the mean number of defects per capacitor. Assuming that the mean time to breakdown for a capacitor with n defects is τ_n ,

$$1/\tau_n = 1/\tau_0 + n/\tau_1$$

where τ_0 and τ_1 are the respective mean times to breakdown for a defect-free capacitor and a capacitor with a single defect. The factor n enters since the mean time associated with n defects is taken as inversely proportional to the area of the defects [25]. A small correction due to reduction of defect-free area, which would alter the $1/\tau_0$ term, is neglected. The expectation value $N_{\rm B}$ for the number of capacitors breaking down within t is

$$N_{\rm B} = N \sum_{n=0}^{\infty} \frac{e^{-\mu} \mu^n}{n!} (1 - e^{-t/\tau_n})$$

$$= N \left[1 - e^{-t/\tau_0} e^{-\mu(1 - e^{-t/\tau_1})} \right]. \tag{8}$$

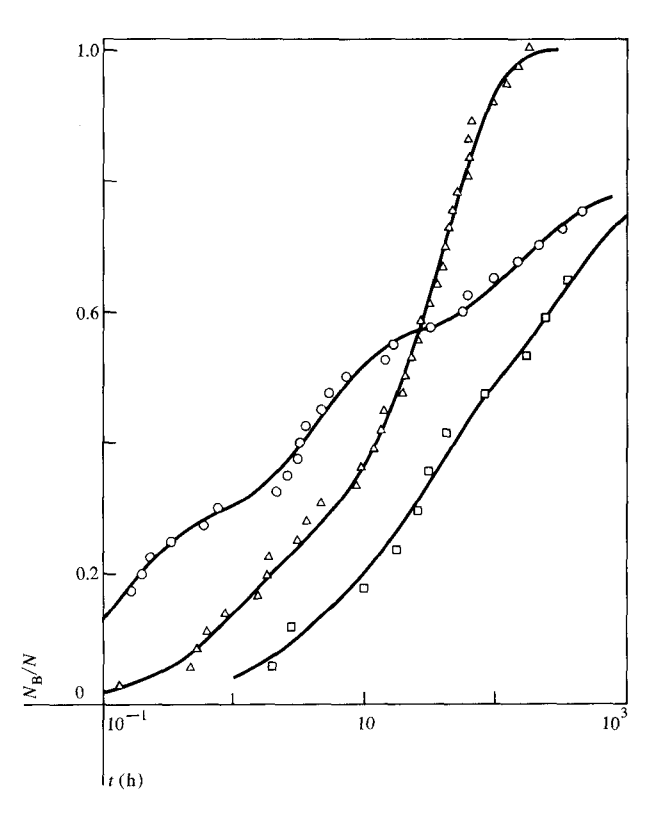


Figure 5 Cumulative number of breakdown events for MOS capacitors with thin oxide films grown at 1200°C and etched back to 36 nm (\square); $T_{ox} = 1000$ °C, grown to 36 nm (\square); and $T_{ox} = 850$ °C, grown to 25 nm (\triangle). The curves represent fits of Eq. (4) to the experimental data with parameters as discussed in the text.

Table 4 Parameter values for three data sets shown in Fig. 5.

T_{ox} (°C)	N_i ; $i =$			τ_i (h); $i =$			
	1	2	3	1	2	3	
1200	2	5	6	3	32.1	350.2	0.35
1000	10	12	9	0.141	5.15	195	0.55
850	8	29		0.85	42.5		0.66

In Figs. 6(a) and (b) we display $N_{\rm B}/N$ as a function of the normalized time $t'=t/\tau_1$ for various values of μ and $r=\tau_1/\tau_0$. The influence of defects on the shapes of the curve is evident and indicates features observed in the data. For large μ , a steep rise is seen and the effect of τ_0 is minimal. The shape for $\mu=4$ is similar to that observed for the capacitors oxidized at 850°C (given in Fig. 5), where we expect the largest defect density or large μ . When μ is near one and r small, a plateau is found; see Fig. 6(b). This plateau arises since with small μ a significant number of capacitors can be defect-free and they will

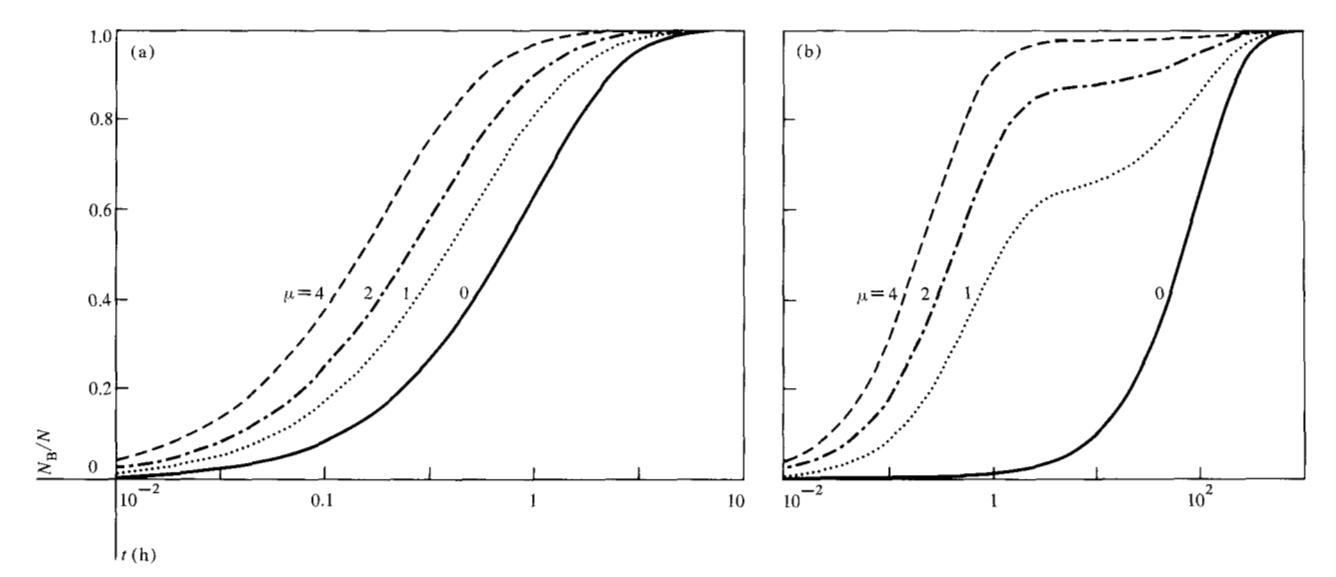


Figure 6 The fraction of samples broken down N_B/N [given by Eq. (8)] as a function of the normalized time $t' = t/\tau_1$ and the average number of defects per sample μ . In (a) $r = \tau_0/\tau_1 = 1$, in (b) r = 0.01.

last significantly longer than defective capacitors when r is small. This type of curve is similar to that observed for the capacitors oxidized at 1000° C that were given in Fig. 5. Thus, Eq. (8) contains the features we observed experimentally; we preferred the analysis of our data given in the section on results and analysis since we did not wish to assume any specific distribution a priori and because our sample sizes were limited.

The yield Y is defined as

$$Y = 1 - N_{\rm B}/N \tag{9}$$

and is commonly assumed [1] to be related to a defect density D, according to

$$Y = e^{-A'D}, (10)$$

where A' is the capacitor area. As pointed out by Solomon [1], D is a function of the field and the time of application of the field. From Eq. (7) we have in our model that

$$Y = e^{-t/\tau_0} e^{-\mu(1 - e^{-t/\tau})},\tag{11}$$

which indicates the field $(\tau_1 \text{ and } \tau_0)$ and time dependences. The actual defect density is μ/A' . For the assumed defect density D to approximate μ/A' , the following inequalities should be satisfied:

$$\tau_1 << t << \mu \tau_0. \tag{12}$$

If low fields are used, $\mu\tau_0$ is expected to be large and the second equality is probably obeyed, but then τ_1 is also large and long times are required for the experiment. At high fields, the problem is that μ is not known prior to the experiment and one cannot be confident that the second inequality is satisfied. Thus, a technique to ascertain a

defect density that does not rely on breakdown is desirable. The conduction method described previously provides such a technique.

In the ramp method, the probability density

$$p = \frac{1}{N} \left(\frac{dN_{\rm B}}{dF} \right) \tag{13}$$

is plotted as a function of the oxide field F and F = Rt, with R being a constant. For this case, Eq. (8) is revised so that

$$\frac{N_{\rm B}}{N} = 1 - Q_0 e^{-\mu(1-Q_1)};$$

$$Q_0 = e^{-\int_0^F \frac{dF'}{R\tau_0}}, \qquad Q_1 = e^{-\int_0^F \frac{dF'}{R\tau_1}}.$$
(14)

If we assume, following Solomon, Klein, and Albert [26], that the dependences of τ_0 and τ_1 on the field are given by

$$\tau_0 = \tau_{00} e^{\frac{-F}{F_{\infty}}}$$
 and $\tau_1 = \tau_{10} e^{\frac{-F}{F_{10}}}$, (15)

we obtain

$$p = \left(1 + \frac{\mu \tau_0 Q_1}{\tau_1}\right) \frac{Q_0}{R \tau_0} e^{-\mu(1-Q_1)};$$

$$Q_0 = e^{-\frac{F_{00}}{R \tau_{00}} \left(e^{\frac{P}{F_{00}}} - 1\right)}, \qquad Q_1 = e^{-\frac{F_{10}}{R \tau_{10}} \left(e^{\frac{P}{F_{10}}} - 1\right)}.$$
(16)

Equations (16) are a generalization of the result of Solomon, Klein, and Albert [26] to the case of a Poisson distribution of defects and reduce to their equation in the absence of defects $(\tau_1 \to \infty)$.

Figures 7(a)-(c) and 8 present the distribution p for choices of the parameters τ_{00} , F_{00} , τ_{10} , F_{10} , and μ , which

476

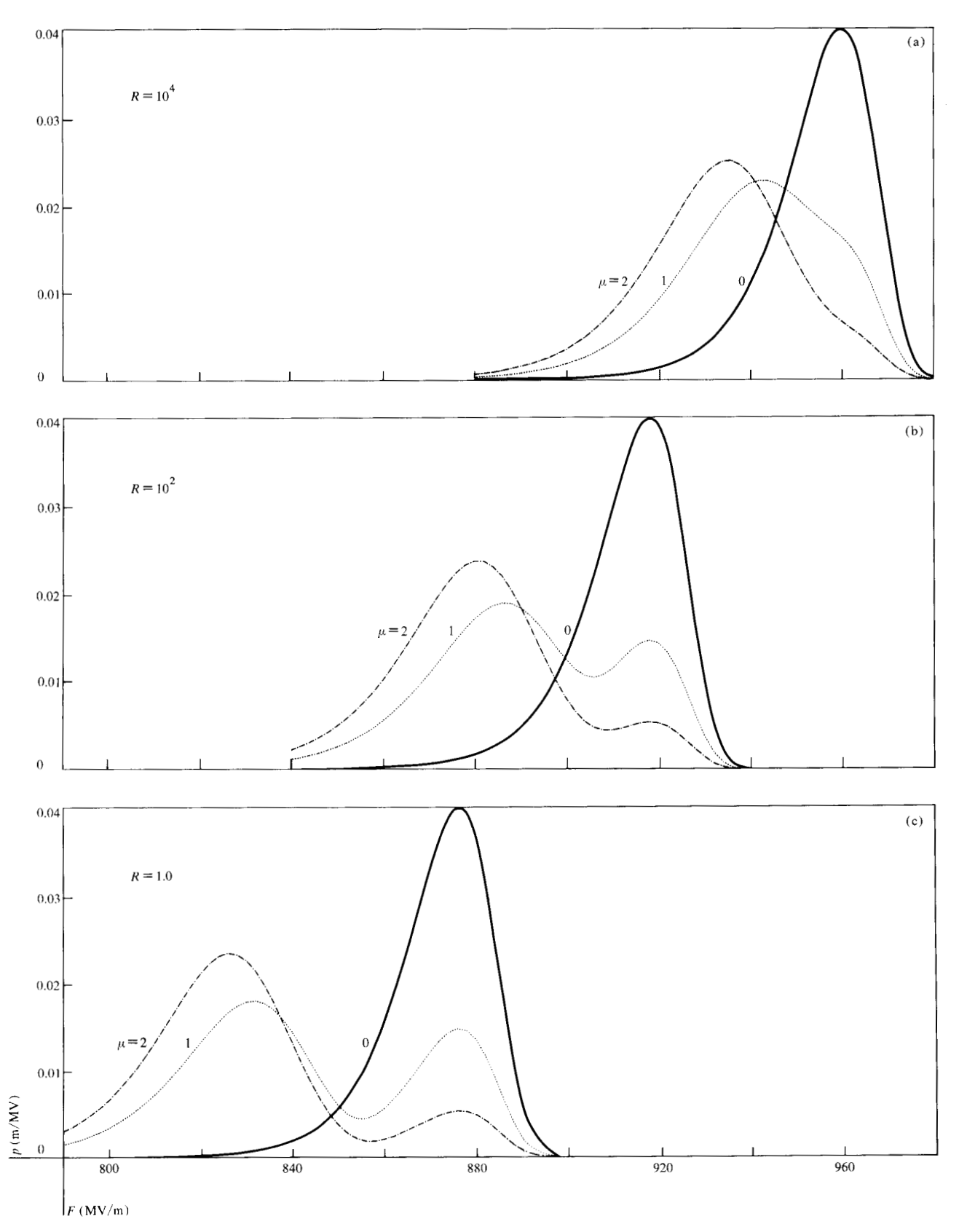


Figure 7 Breakdown probability density p as a function of the field F and μ , as given by Eqs. (16) for various ramp rates R (MV/m-s); $\tau_{00} = 6.7 \times 10^{42}$ s, $\tau_{10} = 6.3 \times 10^{31}$ s, $F_{00} = 9.1$ MV/m, and $F_{10} = 11.8$ MV/m.

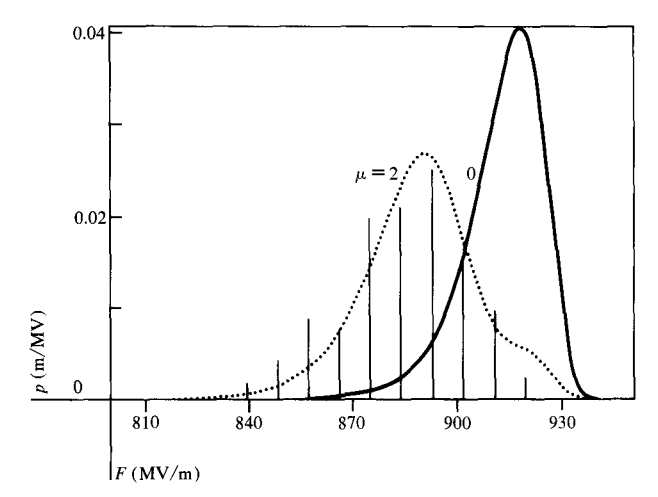


Figure 8 The same as Fig. 7(b) except that $\tau_{10} = 7.28 \times 10^{34}$ s and $F_{10} = 11$ MV/m. Vertical lines are the data of Osburn and Ormond [26] converted to a probability density.

are essentially arbitrary except that in Fig. 8 the combination used essentially fits the data of Osborn and Ormond [27] for R = 100 MV/m-s. The following conclusions can be reached:

- The position of the peak is logarithmically dependent on the ramp rate R, and each of the peaks shifts to higher fields as the ramp rate increases. The shifts are equal for each decade increase in R. This is evident from Figs. 7(a)–(c).
- For small μ and large R, the effect of the defects is to broaden the distribution and shift the peak to lower fields [see Figs. 7(a) and 8]. This feature can account for the width of the distribution found by Osborn and Ormond [27], which could not be explained [1] by the defect-free theory of Solomon, Klein, and Albert [26]. This is clearly shown in Fig. 8. The defect-free ($\mu = 0$) curve is not a good fit to the data of Osborn and Ormond (which we reproduce); however, the $\mu = 2$ curve is a good representation of those data.
- When μ is large and R low, a bimodal distribution is observed [as seen in Figs. 7(b) and (c)]. This is analogous to the distribution observed by Fritzsche [28]. At high R, the defect-related breakdown mode tends to merge into the intrinsic mode.

A wide range of ramp rates are thus desirable in ramp testing. By using only fast ramps, much information concerning defects is lost because defect-induced breakdowns cannot be separated from intrinsic ones. With only slow ramps, if the defect density is large, the intrinsic breakdowns will not be observed.

Acknowledgments

We wish to acknowledge the technical assistance of our coworkers F. Hoev and A. Markle.

References

- P. Solomon, "Breakdown in Silicon Oxide—A Review," J. Vac. Sci. Technol. 14, 1122 (1977).
- 2. W. Kern, "Detection and Characterization of Localized Defects in Dielectric Films," RCA Rev. 34, 655 (1973).
- 3. J. M. Keen, "Nondestructive Optical Technique for Electrically Testing Insulated-Gate Integrated Circuits," *Electron. Lett.* 7, 432 (1971).
- 4. R. Williams and M. H. Woods, "Laser-Scanning Photoemission Measurements of the Silicon-Silicon Dioxide Interface," J. Appl. Phys. 43, 4142 (1972).
- T. H. DiStefano, "Dielectric Breakdown Induced by Sodium in MOS Structures," J. Appl. Phys. 44, 527 (1973);
 "Barrier Inhomogeneities and Si-SiO₂ Interfaces by Scanning Internal Photoemission," Appl. Phys. Lett. 19, 280 (1971).
- J. W. Philbrick and T. H. DiStefano, "Scanned Surface Photovoltage Detection of Defects in Silicon Wafers," Proceedings of the 13th Annual Reliability Physics Conference, Las Vegas, April 1, 1975, p. 159.
- T. H. DiStefano, "Photoemission and Photovoltaic Imaging of Semiconductor Surfaces," NBS Special Publication 400-23, ARPA/NBS Workshop IV, Gaithersburg, Maryland, April 23-24, 1975, National Bureau of Standards, Washington, DC.
- M. Av-Ron, M. Shatzkes, T. H. DiStefano, and I. Cadoff, "The Nature of Electron Tunneling in SiO₂," The Physics of SiO₂ and its Interfaces, S. T. Pantelides, Ed., Pergamon Press, Elmsford, NY, 1978, p. 45.
- M. Av-Ron, M. Shatzkes, T. H. DiStefano, and R. A. Gdula, "On Al-SiO₂ Interfaces and Oxidation Temperatures," Proceedings of the 11th International Conference on Semiconductor Devices, Tokyo, Japan, August 27-29, 1979, to be published by Jpn. J. Appl. Phys.
- C. M. Osburn and N. J. Chou, "Accelerated Dielectric Breakdown of Silicon Dioxide Films," J. Electrochem. Soc. 120, 1377 (1973).
- C. M. Osburn and E. Bassous, "Improved Dielectric Reliability of SiO with Polycrystalline Silicon Electrodes," J. Electrochem. Soc. 122, 89 (1975).
- J. M. Green, C. M. Osburn, and T. O. Sedgwick, "The Influence of Silicon Heat Treatments on the Minority Carrier Generation and Dielectric Breakdown in MOS Structures,"
 J. Electron. Mater. 3, 579 (1974).
- C. M. Osburn and D. W. Ormond, "Dielectric Breakdown in SiO₂ Films on Si: II. Influence of Processing and Materials," J. Electrochem. Soc. 119, 597 (1972).
- M. Shatzkes and M. Av-Ron, "Impact Ionization and Positive Charge in Thin SiO₂ Films," J. Appl. Phys. 47, 3192 (1976).
- 15. C. M. Osburn and E. J. Weitzman, "Electrical Conduction and Dielectric Breakdown in Silicon Dioxide Films on Silicon," *J. Electrochem. Soc.* 119, 603 (1972).
- H. L. Hughes, R. D. Baxter, and B. Phillips, "Dependence of MOS Device Radiation-Sensitivity on Oxide Impurities," *IEEE Trans. Nucl. Sci.* NS-19, 256 (1972).
- F. M. Fowkes and F. E. Witherell, "Sodium Mobility in Irradiated SiO₂," *IEEE Trans. Nucl. Sci.* NS-21, 67 (1974).
- J. R. Srour, O. L. Curtis, and K. Y. Chiu, "Charge Transport Studies in SiO₂: Processing Effects and Implications for Irradiation Hardening," *IEEE Trans. Nucl. Sci.* NS-21, 73 (1974).
- 19. D. R. Kerr, "MIS Measurement Technique Utilizing Slow-Voltage RAMPs," Proceedings of the International Conference on the Use of MIS Structures, Grenoble, France, June

- 17-20, 1969, J. Borel, Ed., Centre d'Etudes Nucléaires de Grenoble, LETI, Grenoble, 1969, pp. 303-315.
- A. S. Grove, B. E. Deal, E. H. Snow, and C. T. Sah, "Investigation of Thermally Oxidized Silicon Surfaces Using Metal-Oxide-Semiconductor Surfaces," Solid-State Electron. 8, 145 (1965).
- R. Williams, "Injection by Internal Photoemission," Semiconductors and Semimetals, Vol. 6, R. K. Willardson and A. C. Beer, Eds., Academic Press, Inc., New York, 1970, pp. 93-139.
- R. Williams and M. H. Woods, "High Electric Fields in Silicon Dioxide Produced by Corona Charging," J. Appl. Phys. 44, 1026 (1973).
- L. E. Murphy and R. H. Good, Jr., "Thermionic Emission, Field Emission, and the Transition Region," *Phys. Rev.* 102, 1464 (1956).
- W. Franz, Handbuch Der Physik, Vol. 17, S. Flugge, Ed., Springer, Berlin, 1956, p. 115.

- N. Klein, "Theory of Localized Electron Breakdown in Insulating Films," Adv. Phys. 21, 605 (1972).
 P. Solomon, N. Klein, and M. Albert, "A Statistical Model
- P. Solomon, N. Klein, and M. Albert, "A Statistical Model for STEP and RAMP Voltage Breakdown Tests in Thin Insulators," Thin Solid Films 35, 321 (1976).
- C. M. Osburn and D. W. Ormond, "Dielectric Breakdown in SiO₂ Films on Si: I. Measurement and Interpretation," J. Electrochem. Soc. 119, 591 (1972).
- C. Fritzsche, "Dielectric Breakdown in SiO₂ Layers on Silicon," Z. Angew Phys. 24, 49 (1967).

Received May 31, 1979; revised January 17, 1980

The authors are located at the IBM Data Systems Division laboratory, East Fishkill (Hopewell Junction), New York 12533.